Supporting Information

Nickel-Exchanged Zincosilicate Catalysts for the Oligomerization of Propylene

Mark A. Deimund, Jay Labinger and Mark E. Davis*

Division of Chemistry & Chemical Engineering, California Institute of Technology, Pasadena, CA 91125, United States

*Corresponding author information

Mark E. Davis

Division of Chemistry and Chemical Engineering
California Institute of Technology
Spalding Laboratory
MC 210-41
Pasadena, CA 91125
Tel.: (626) 395- 4251
E-Mail: mdavis@cheme.caltech.edu

*Corresponding author: mdavis@cheme.caltech.edu

Characterization of Materials Used as Catalysts

All materials (with the exception of USY) were synthesized in-house. The powder X-ray diffraction (XRD) patterns for each of these materials as made, after nickel exchange, and after calcination are shown in the following figures.

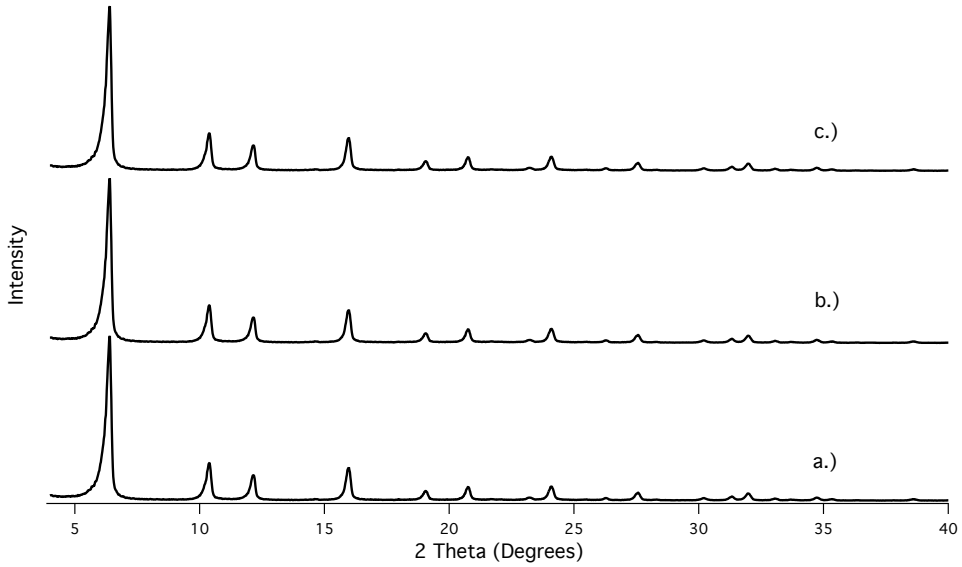

Figure S1. XRD Patterns of a.) As-Received USY, b.) Ni-USY, and c.) Calcined Ni-USY

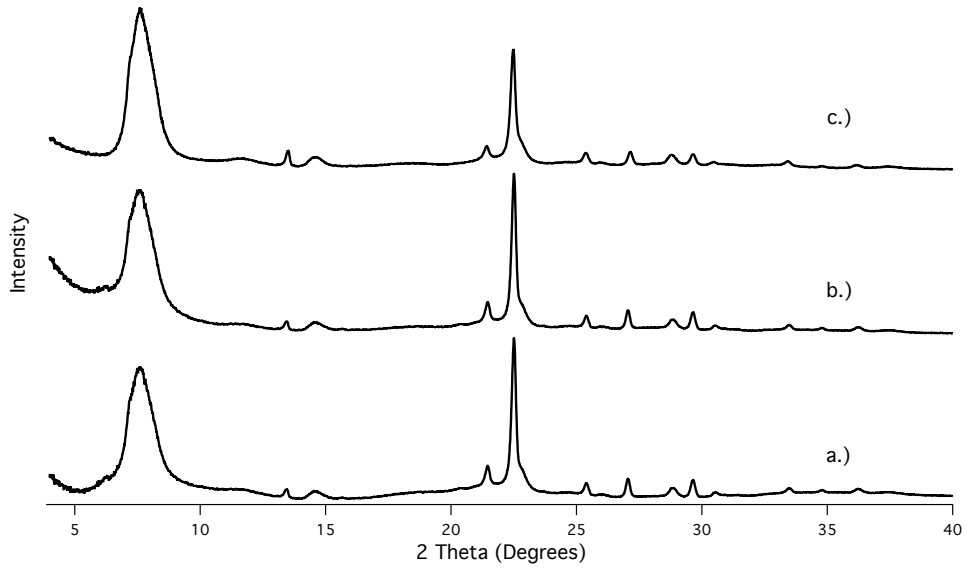

Figure S2. XRD Patterns of a.) As-Made CIT-6, b.) Ni-CIT-6, and c.) Calcined Ni-CIT-6

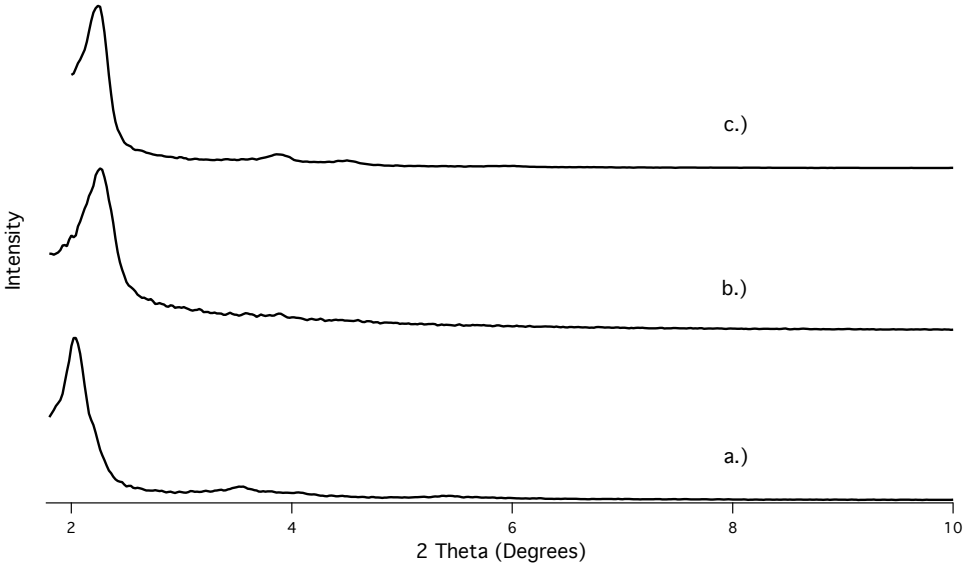

Figure S3. XRD Patterns of a.) As-Made Zn-MCM-41, b.) Ni-Zn-MCM-41, and c.) Calcined Ni-Zn-MCM-41

The high-aluminum zeolite beta (HiAl BEA) was synthesized according to a seeded procedure similar to that described by Majano et al.[21] The XRD patterns for the zeolite beta seeds and resulting solid as made, after nickel exchange, and after calcination are shown below:

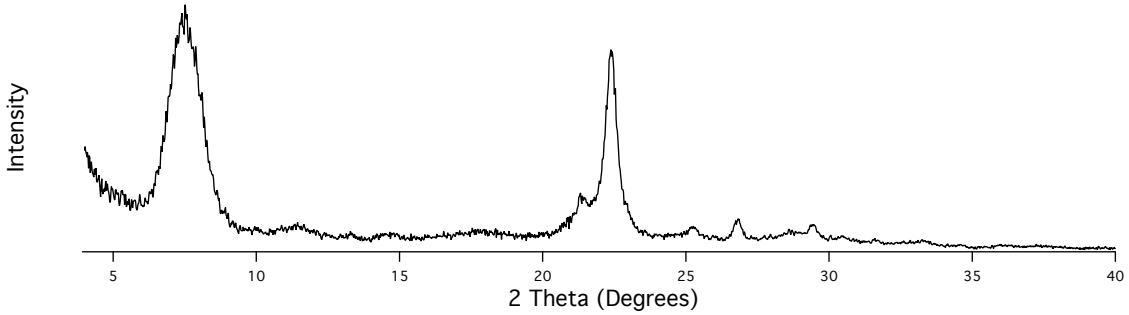

Figure S1. XRD Pattern of Tosoh Zeolite Beta Used As Seeds

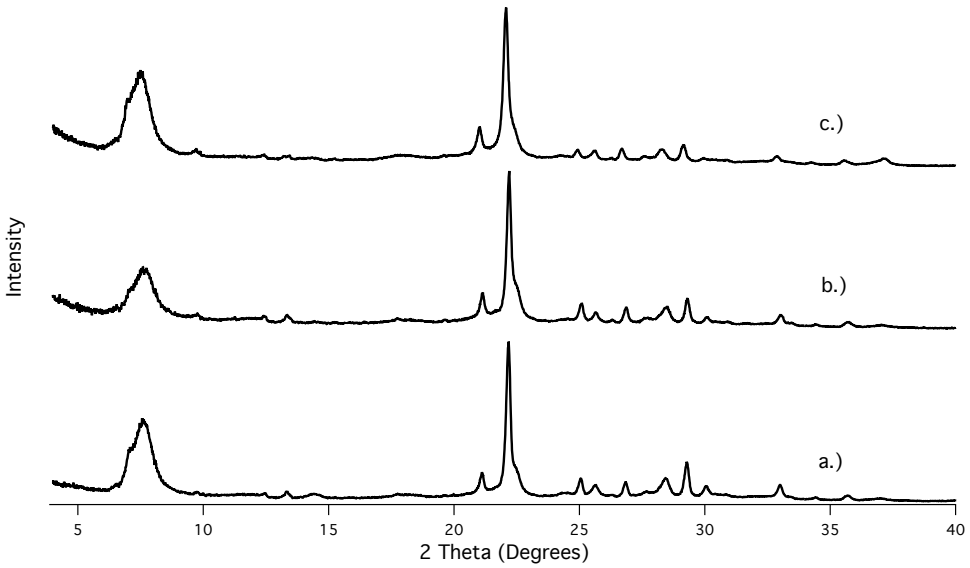

Figure S5. XRD Patterns of a.) As-Made HiAl-BEA, b.) Ni-HiAl-BEA, and c.) Calcined Ni-HiAl-BEA

Additionally, a solid-state ^{27}Al NMR experiment was conducted to confirm that all aluminum atoms in HiAl BEA were tetrahedrally coordinated within the zeolite framework. The NMR spectrum is shown below:

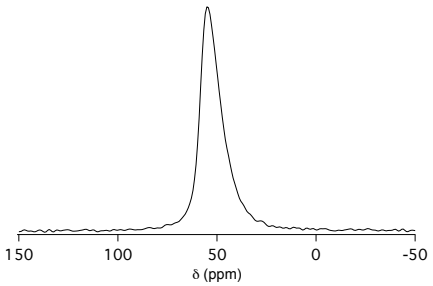

Figure S2. ^{27}Al NMR of HiAl BEA

The peak centered near 50 ppm is characteristic of aluminum atoms in tetrahedral coordination, suggesting all aluminum was incorporated into the zeolite framework.[21-23] No other peaks were observed in the ^{27}Al NMR spectrum.

To determine micropore volume, Ar adsorption was performed on each sample at 87.45 K with a Quantachrome Autosorb iQ adsorption instrument using a constant-dose method. Samples were off-gassed at 80 °C for 1 h, followed by 3 h at 120 °C and 10 h at 350 °C prior to adsorption measurements. Table S.1 displays the pore volumes for each material in the Ni^{2+}-exchanged, calcined form (determined using the t-plot method).

Table S1. Pore Volumes for Materials

Material	**Micropore Volume [cc/g]**
Ni-CIT-6	0.18
Ni-HiAl-BEA	0.16
Ni-USY	0.22
	Pore Volume [cc/g]
Ni-Zn-MCM-41	0.53

Argon adsorption isotherms for each material after Ni^{2+} exchange and calcination are shown below.

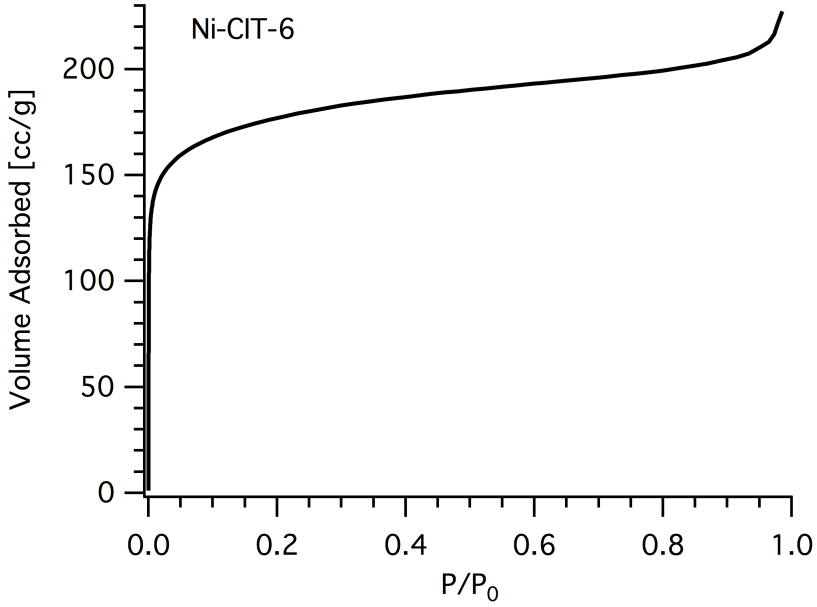

Figure S7. Argon adsorption isotherm for Ni-CIT-6.

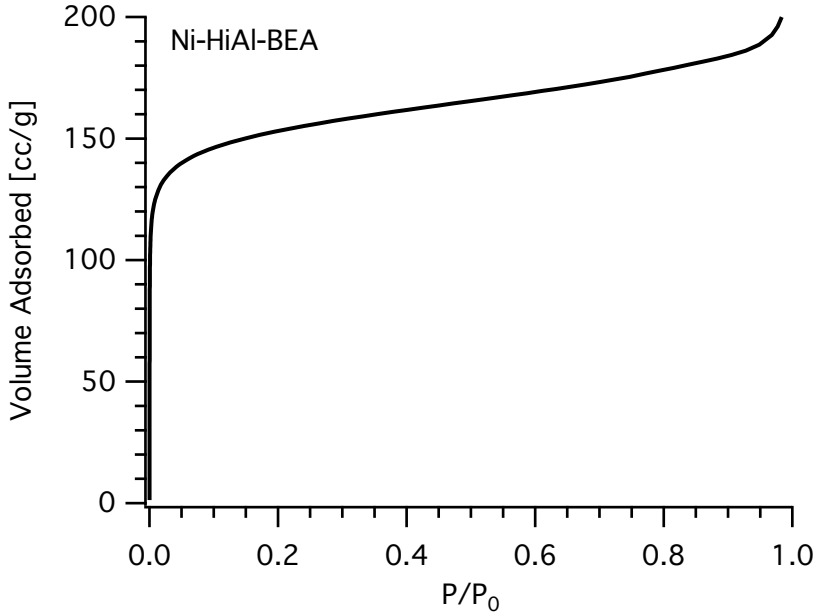

Figure S8. Argon adsorption isotherm for Ni-HiAl-BEA.

The calculated micropore volume for Ni-HiAl-BEA (0.16 cc/g) is lower than expected for a typical *BEA sample, although this micropore volume is consistent with that reported by Kamimura *et al.* for a calcined high-aluminum *BEA sample.[22]

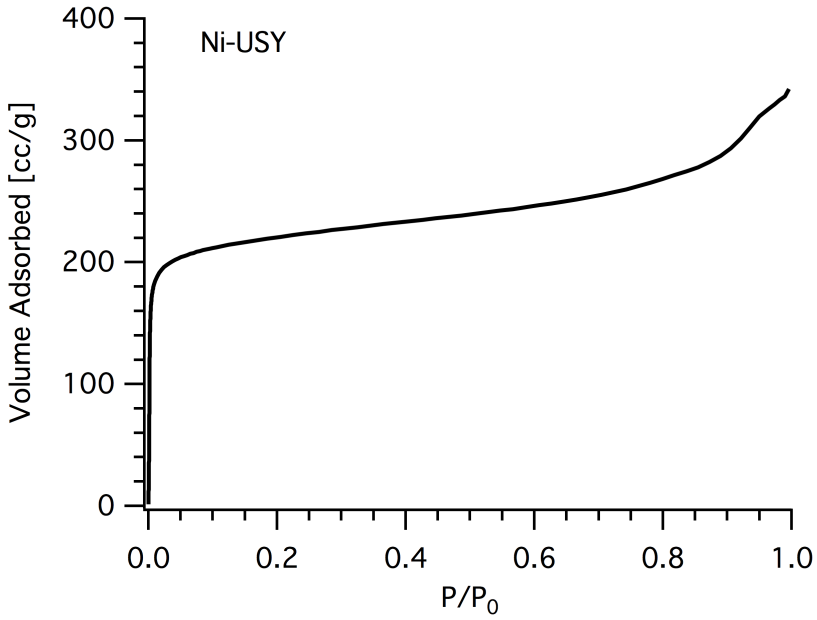

Figure S9. Argon adsorption isotherm for Ni-USY.

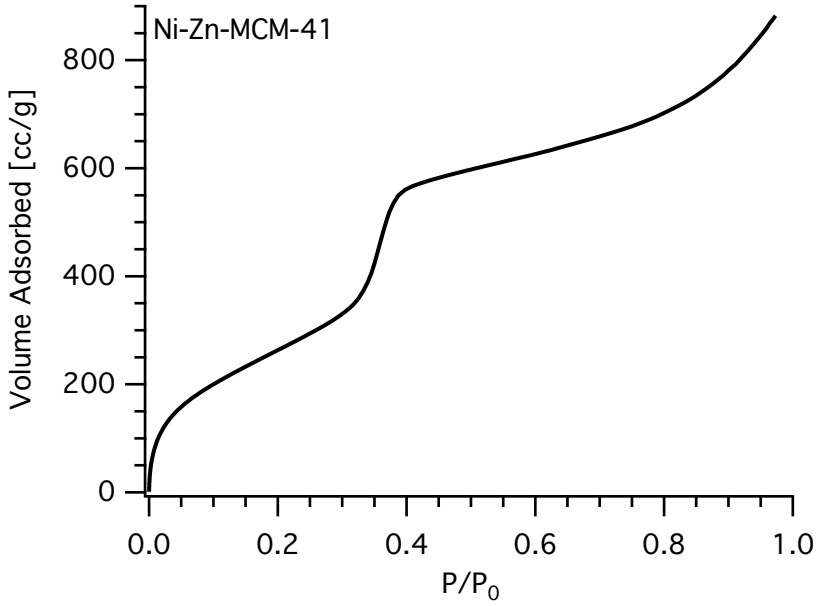

Figure S10. Argon adsorption isotherm for Ni-Zn-MCM-41.

The results of the NH_3 TPD experiments are shown below for each nickel-exchanged, calcined material.

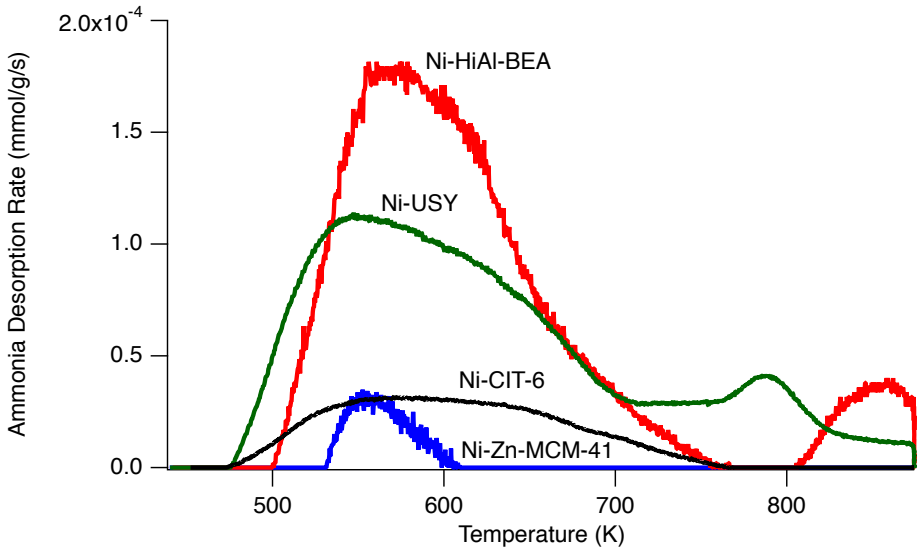

Figure S11. Ammonia TPD for Nickel-Exchanged, Calcined Samples

Mass-spectrometer signal quantification also allowed for determination of the Brønsted acid site concentration for each material. Table S2 below shows these acid site concentrations, which are consistent with the elemental analyses determined previously.

Table S2. Brønsted Acid Site Concentrations for the Nickel-Containing Materials

Material	Acid Site Concentration [mmol/g]
Ni-CIT-6	0.18
Ni-Zn-MCM-41	0.04
Ni-HiAl-BEA	0.73
Ni-USY	0.68

Reaction Data at Two Reaction Temperatures

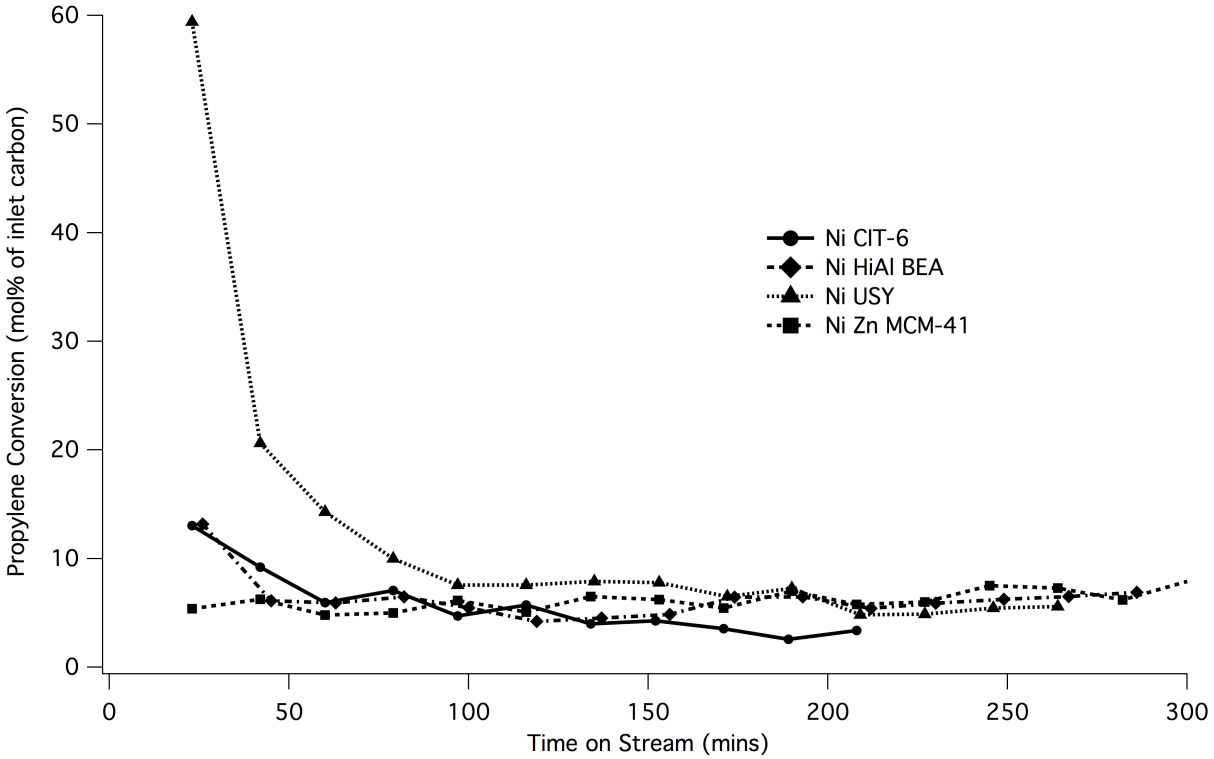

Figure S12. Propylene Conversion vs. TOS for All Catalysts at 180 °C

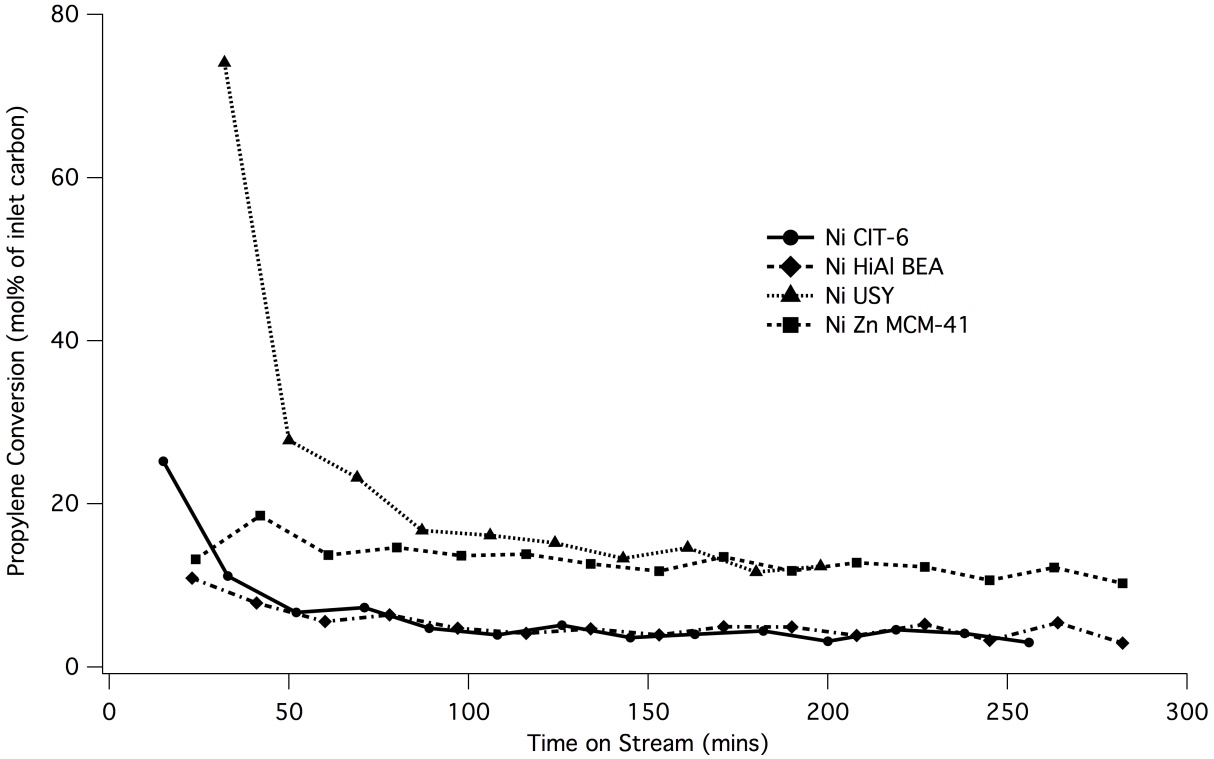

Figure S13. Propylene Conversion vs. TOS for All Catalysts at 250 °C

Complete Selectivity Graphs for All Reaction Runs

Note: Run 1 and Run 2 designate catalyst testing before and after regeneration by calcination in air, respectively.

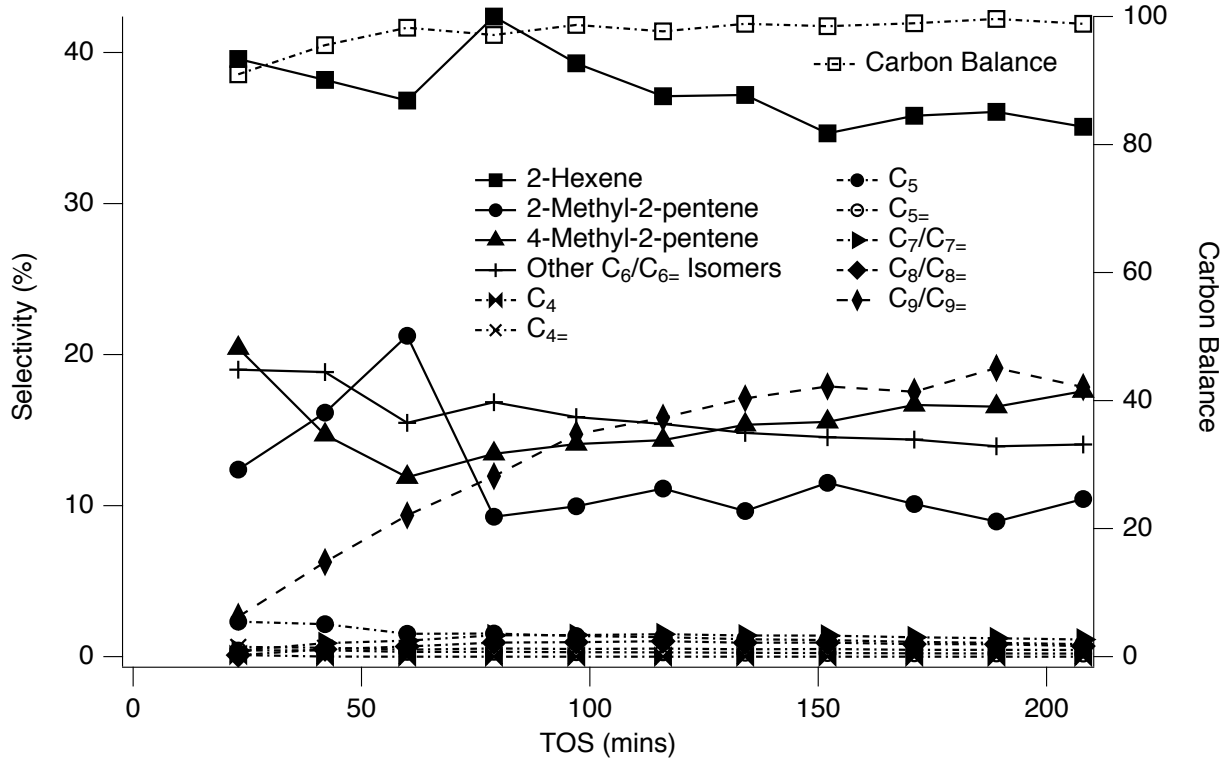

Figure S14. All Selectivities vs. TOS for Run #1 Ni-CIT-6 at 180 °C

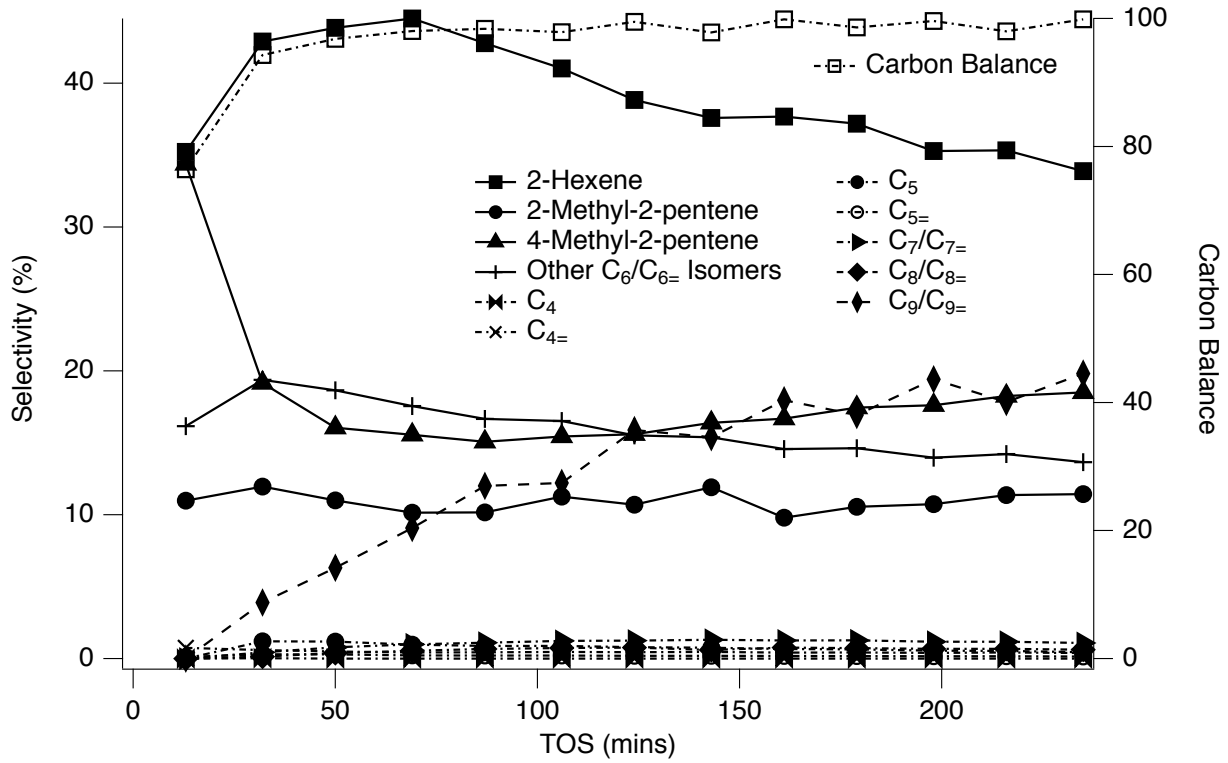

Figure S15. All Selectivities vs. TOS for Run #2 Ni-CIT-6 at 180 °C

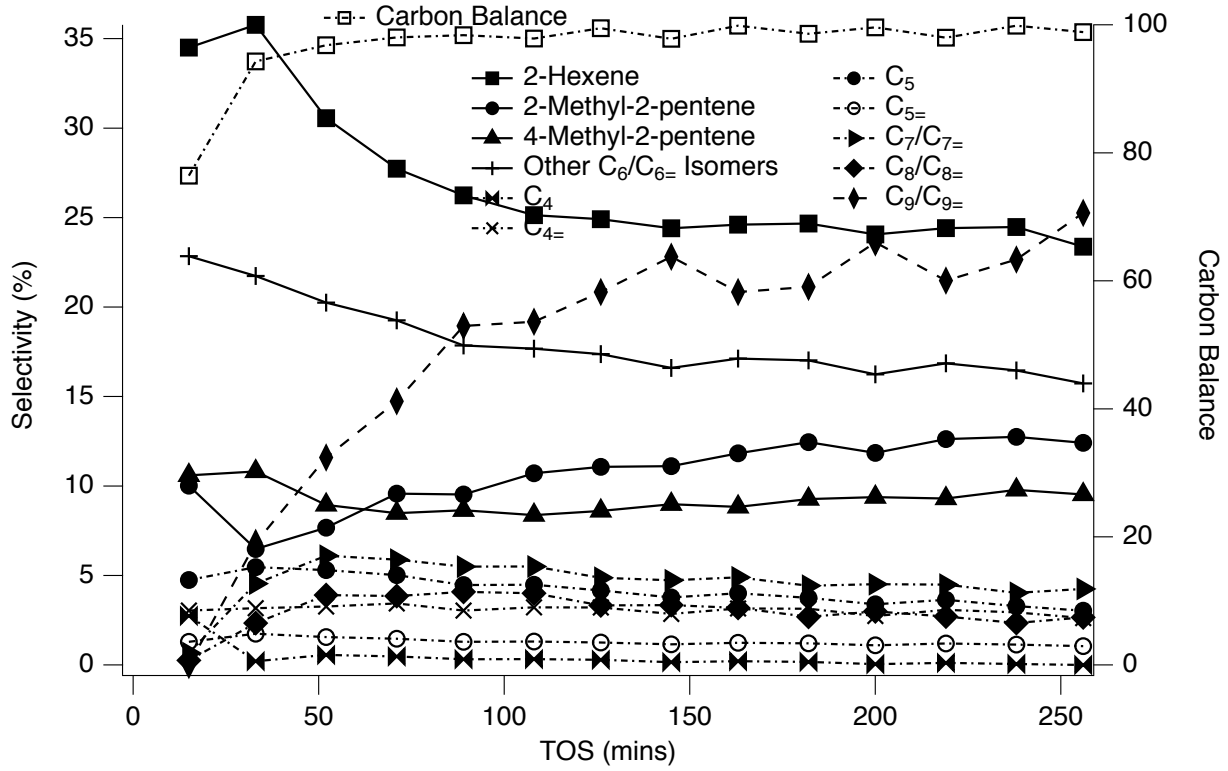

Figure S16. All Selectivities vs. TOS for Run #1 Ni-CIT-6 at 250 °C

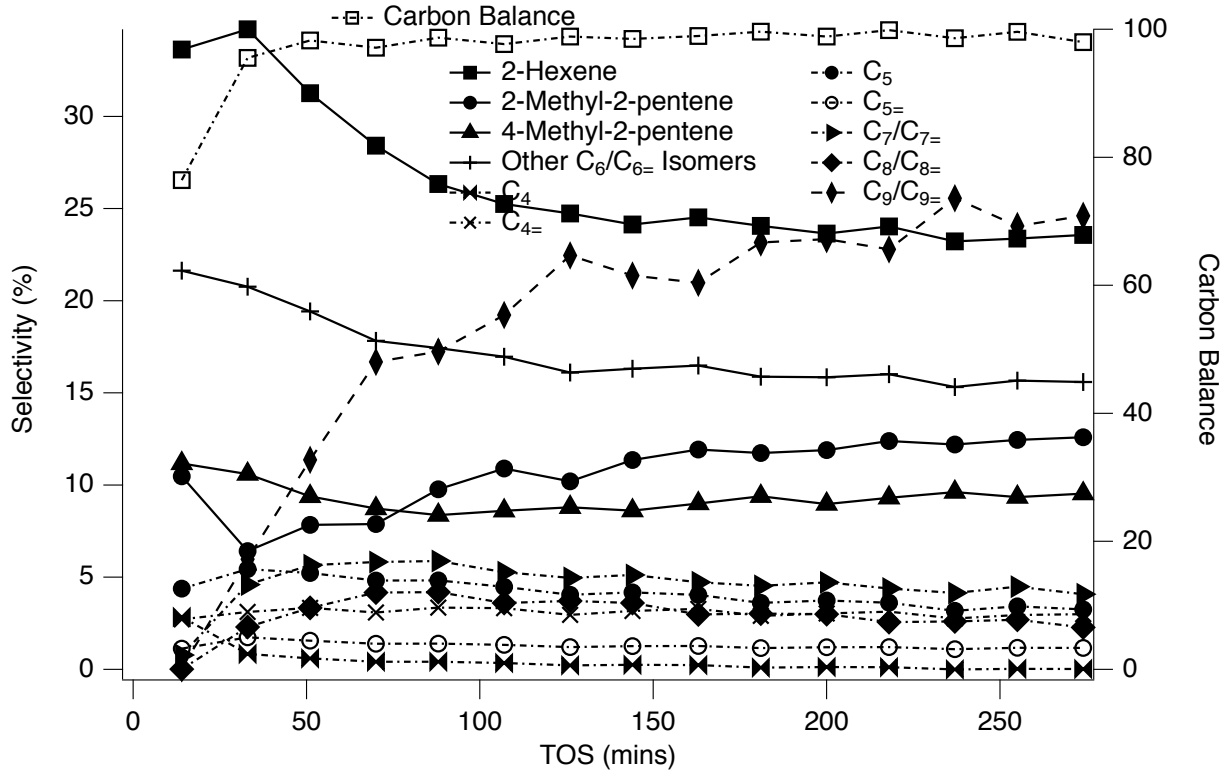

Figure S17. All Selectivities vs. TOS for Run #2 Ni-CIT-6 at 250 °C

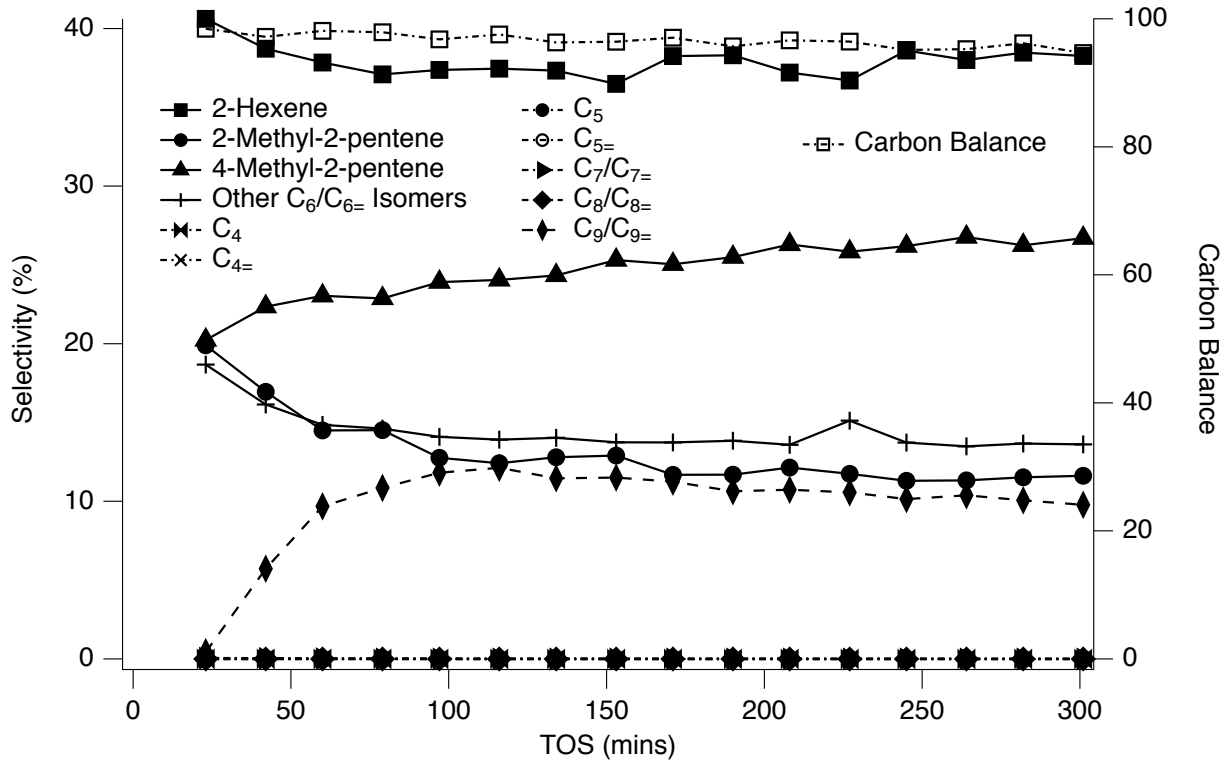

Figure S18. All Selectivities vs. TOS for Run #1 Ni-Zn-MCM-41 at 180 °C

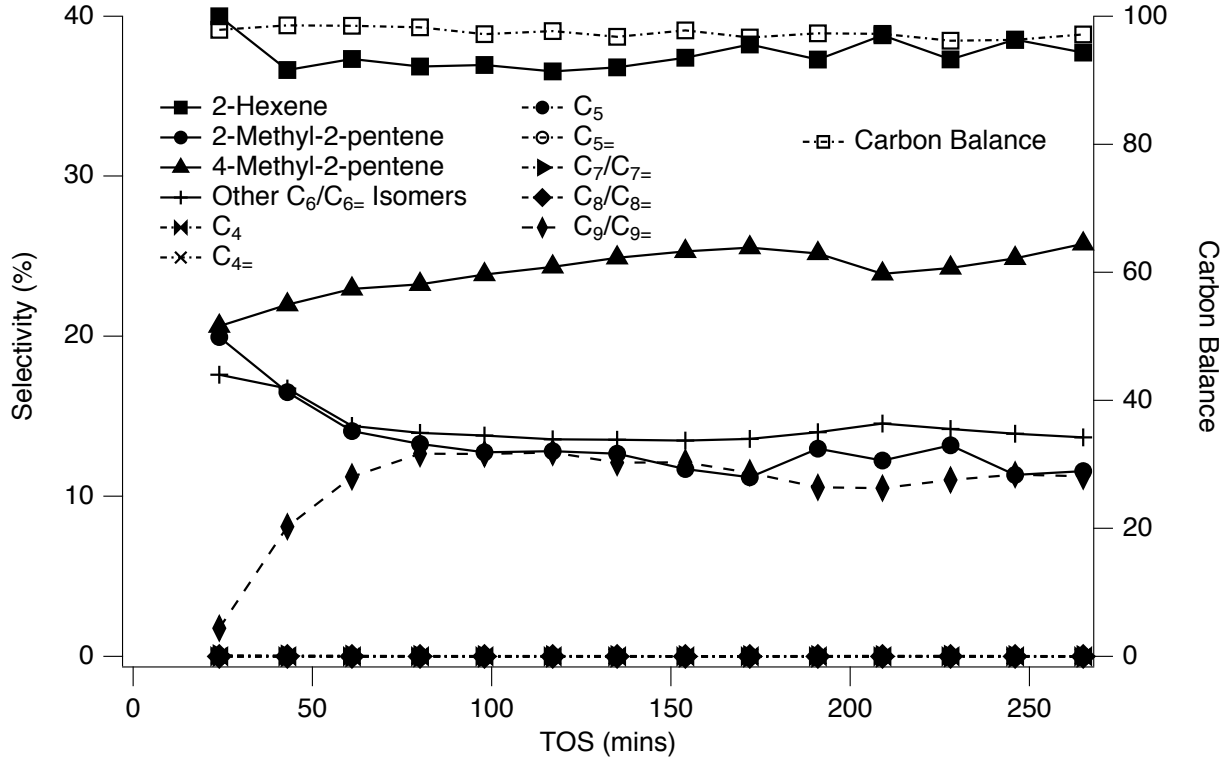

Figure S19. All Selectivities vs. TOS for Run #2 Ni-Zn-MCM-41 at 180 °C

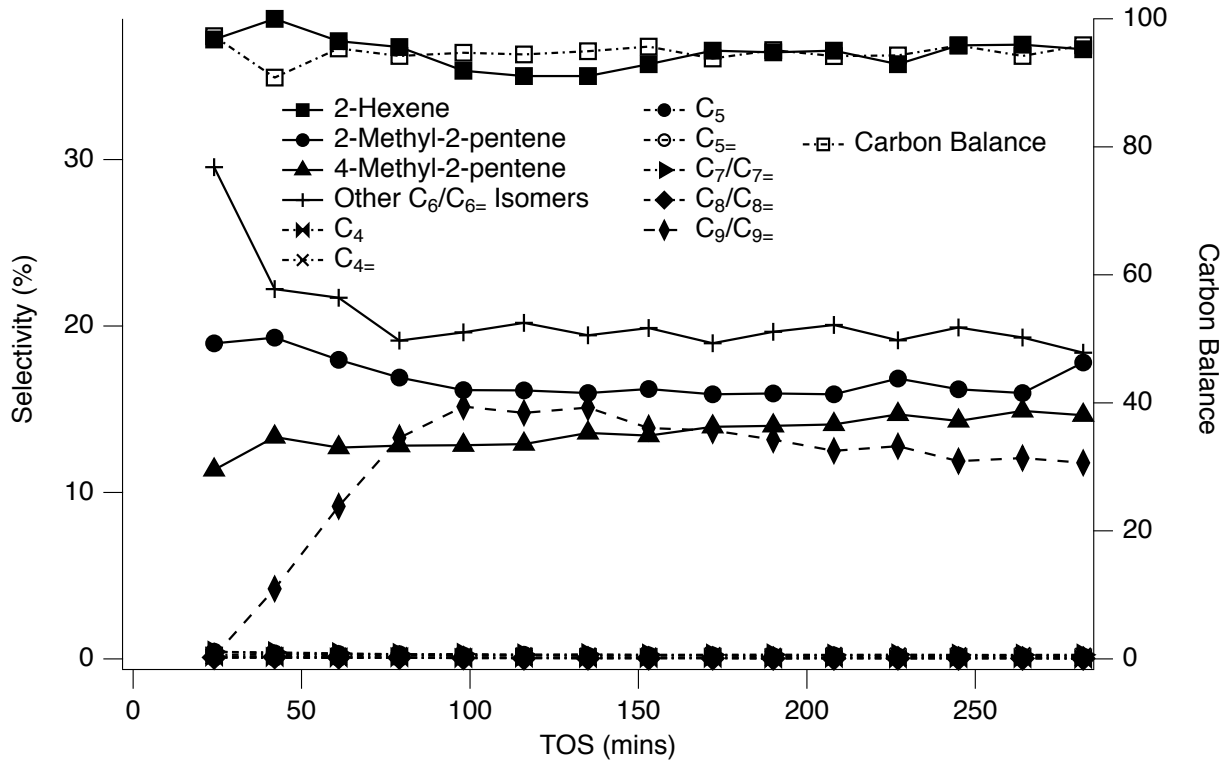

Figure S20. All Selectivities vs. TOS for Run #1 Ni-Zn-MCM-41 at 250 °C

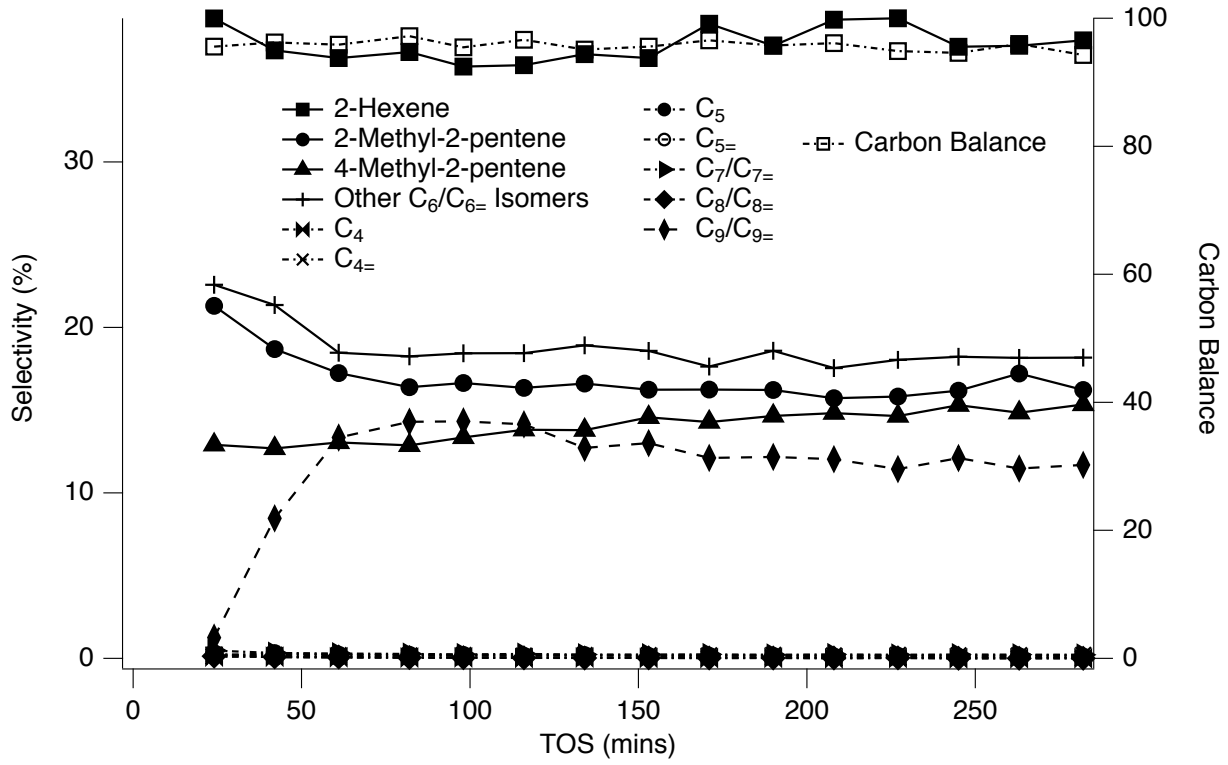

Figure S21. All Selectivities vs. TOS for Run #2 Ni-Zn-MCM-41 at 250 °C

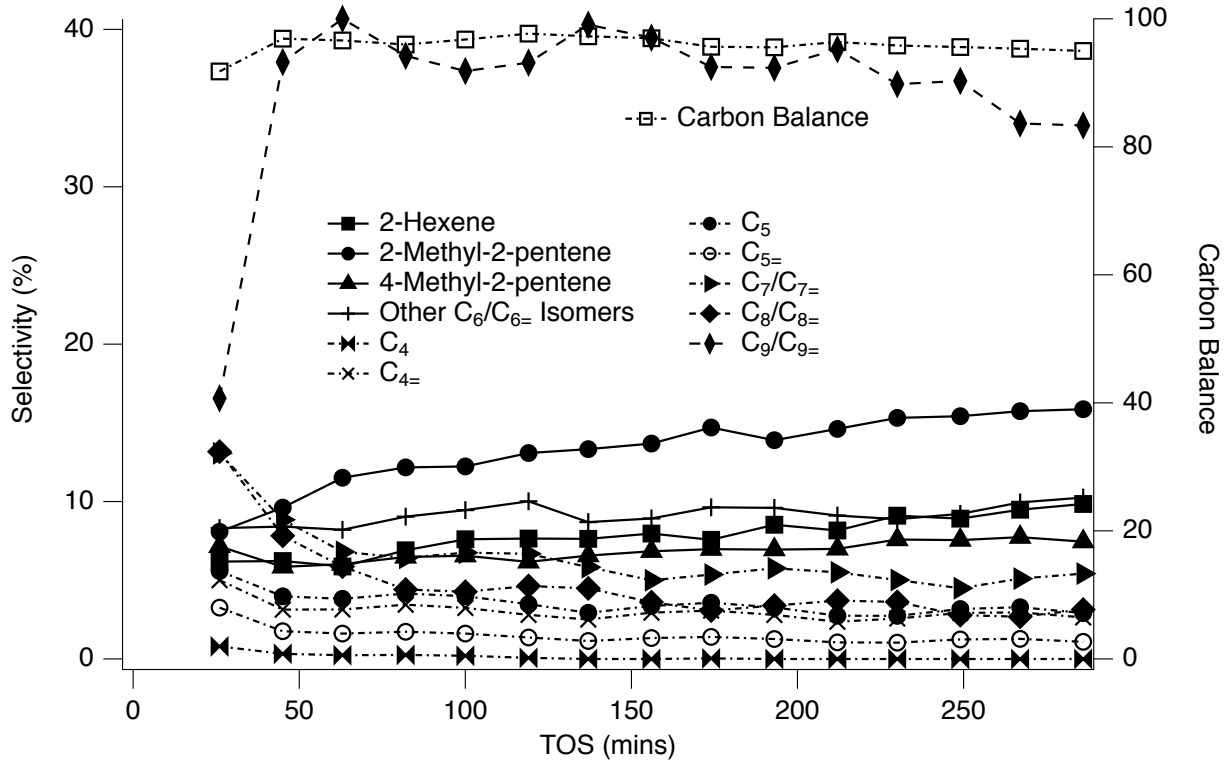

Figure S22. All Selectivities vs. TOS for Run #1 Ni-HiAl-BEA at 180 °C

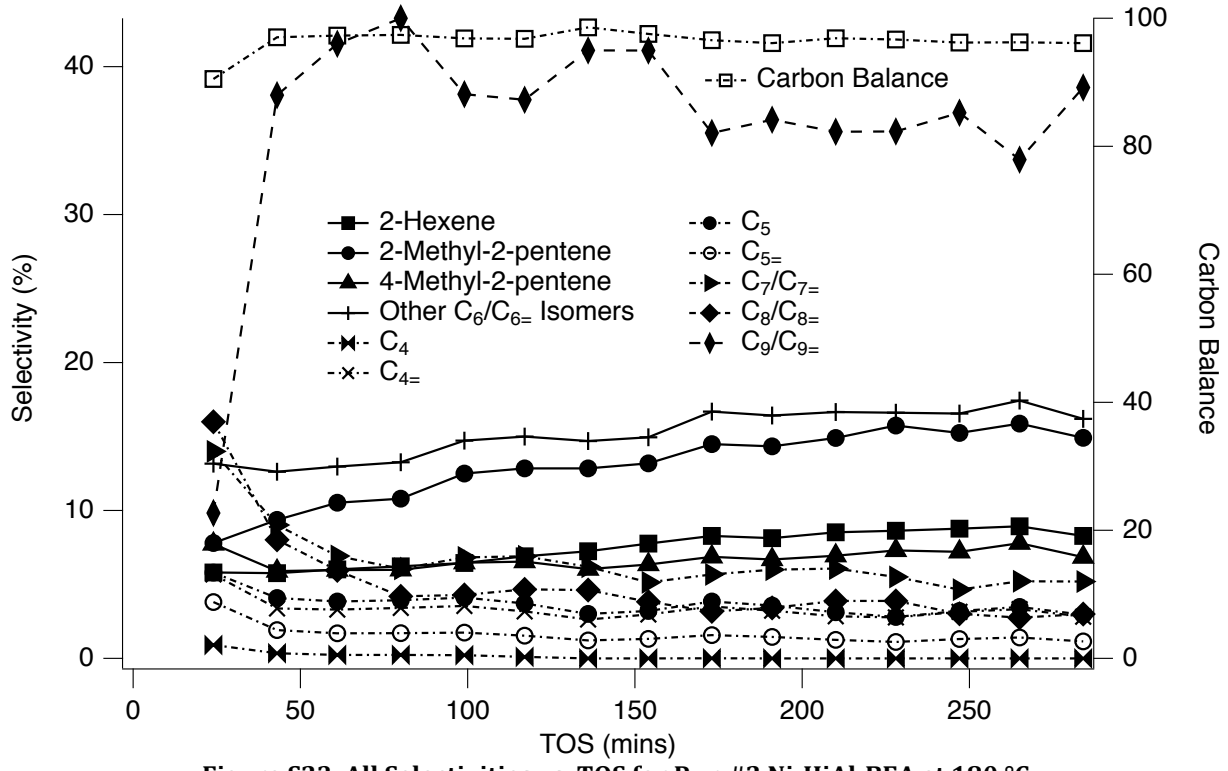

Figure S23. All Selectivities vs. TOS for Run #2 Ni-HiAl-BEA at 180 °C

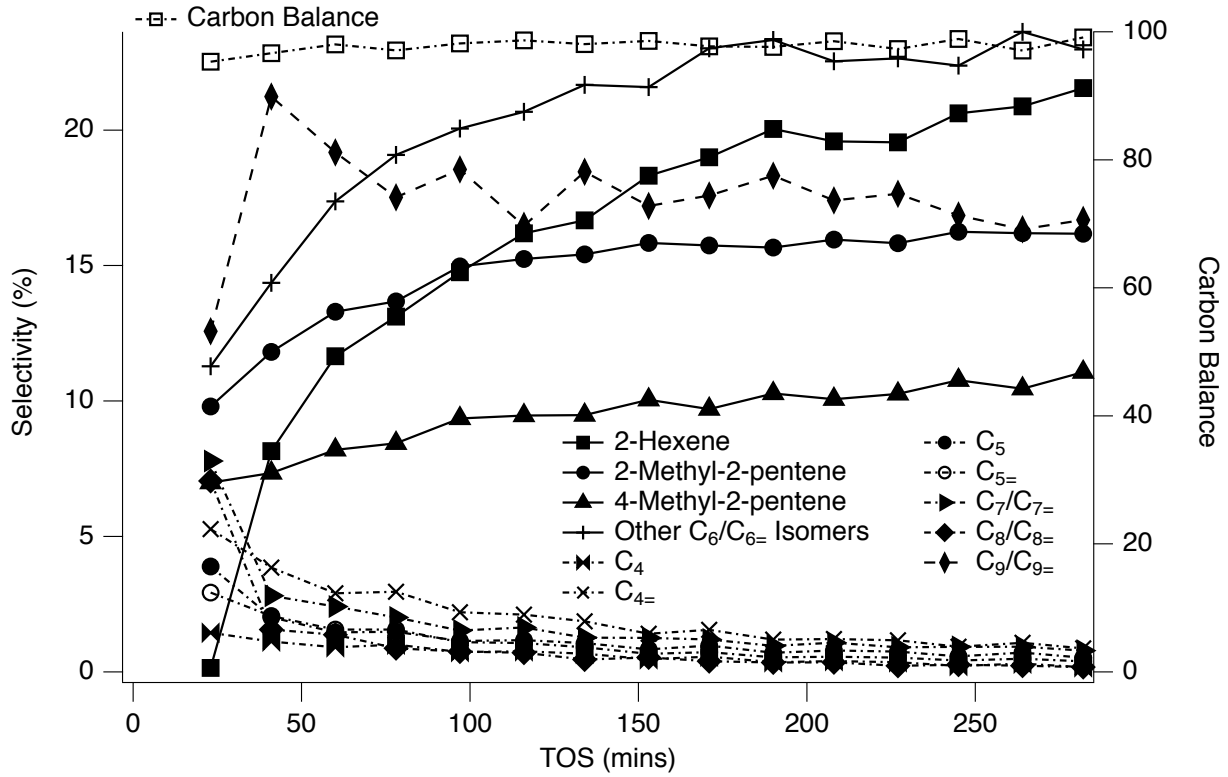

Figure S24. All Selectivities vs. TOS for Run #1 Ni-HiAl-BEA at 250 °C

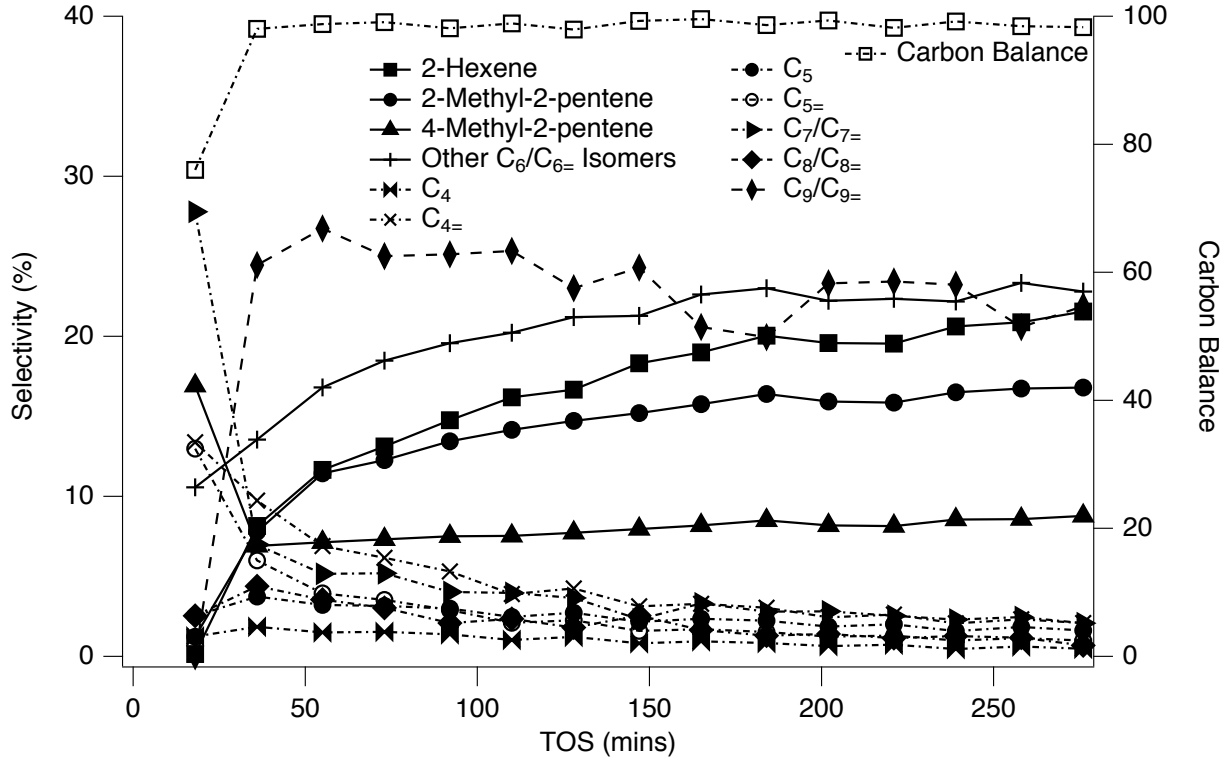

Figure S25. All Selectivities vs. TOS for Run #2 Ni-HiAl-BEA at 250 °C

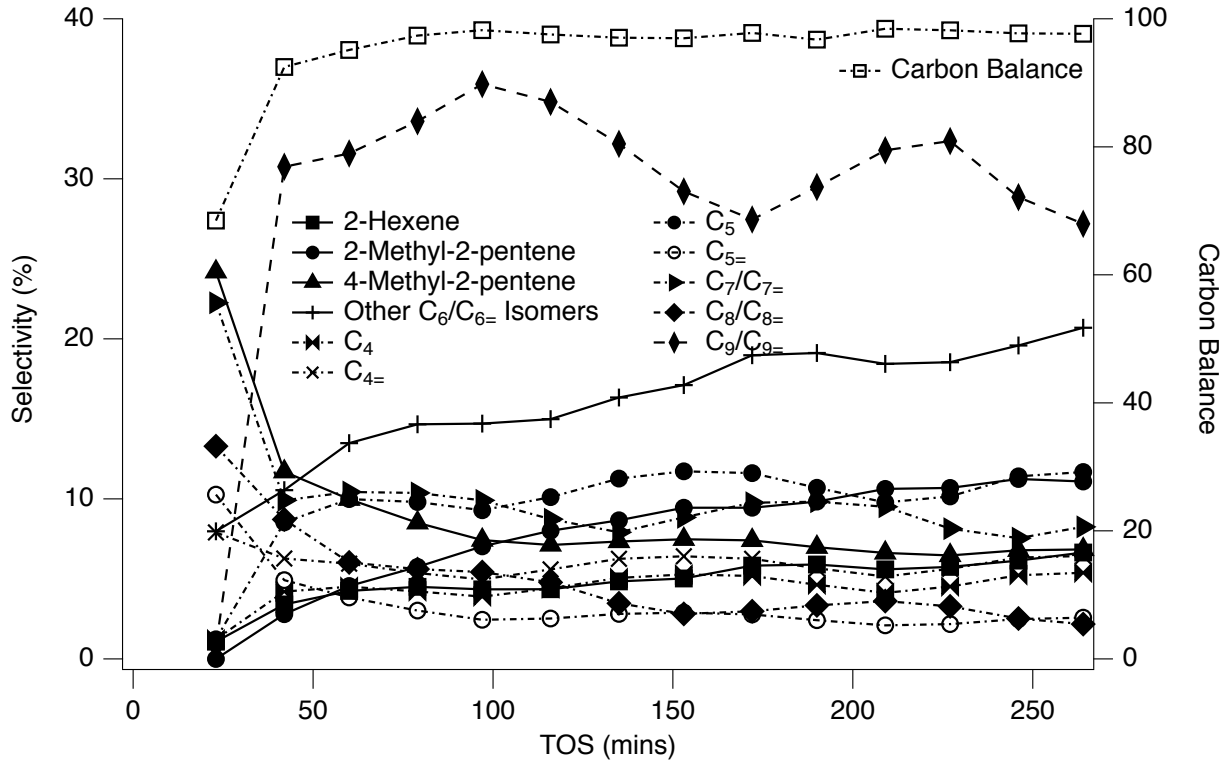

Figure S26. All Selectivities vs. TOS for Run #1 Ni-USY at 180 °C

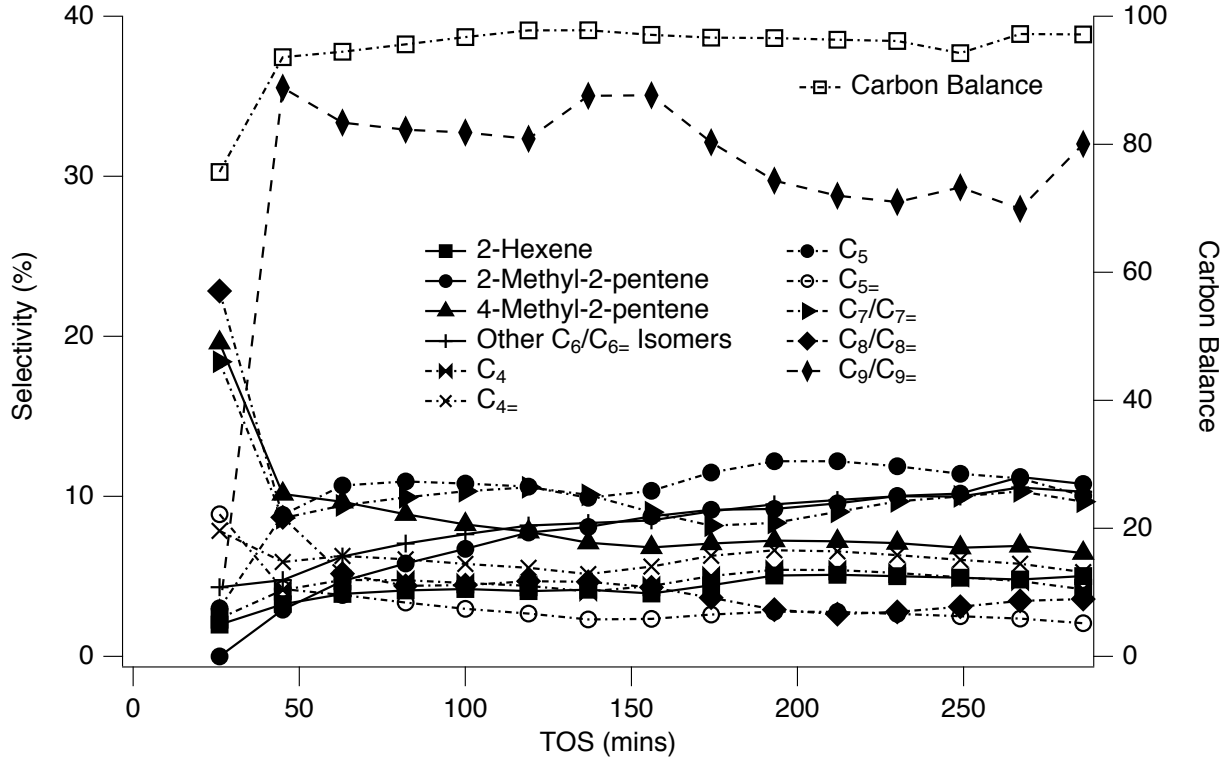

Figure S27. All Selectivities vs. TOS for Run #2 Ni-USY at 180 °C

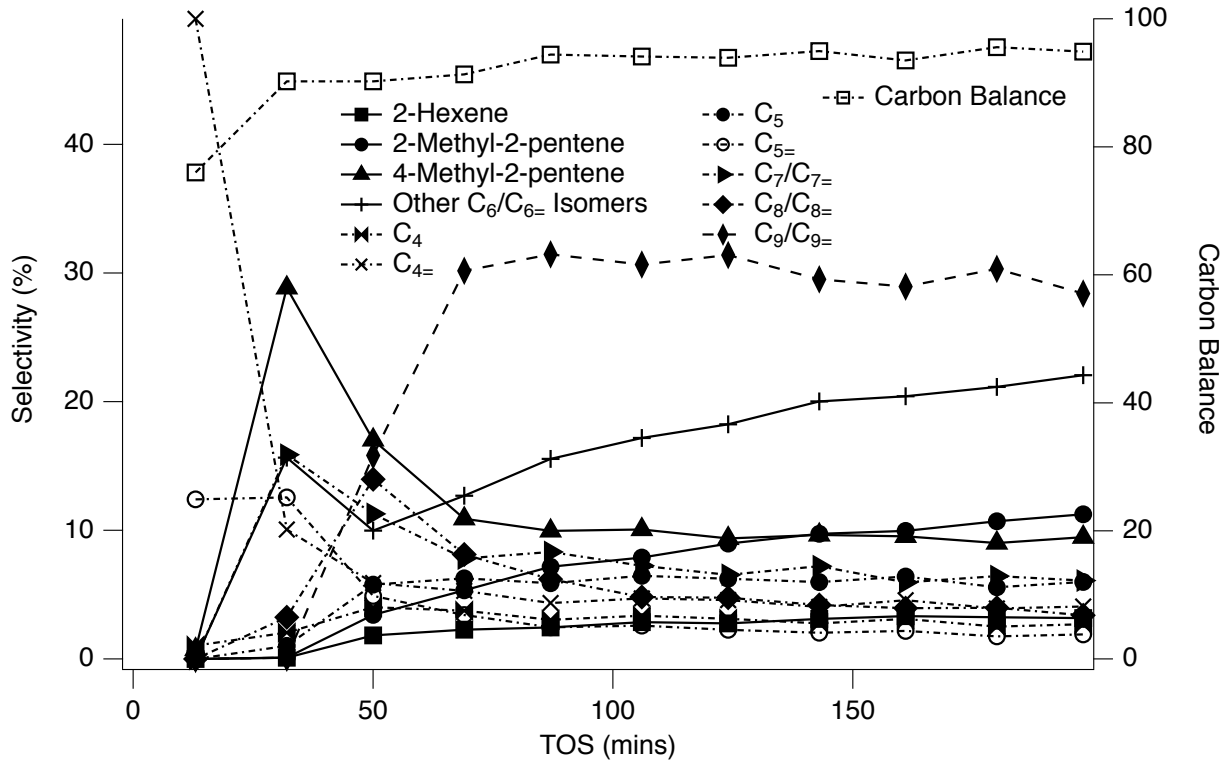

Figure S28. All Selectivities vs. TOS for Run #1 Ni-USY at 250 °C

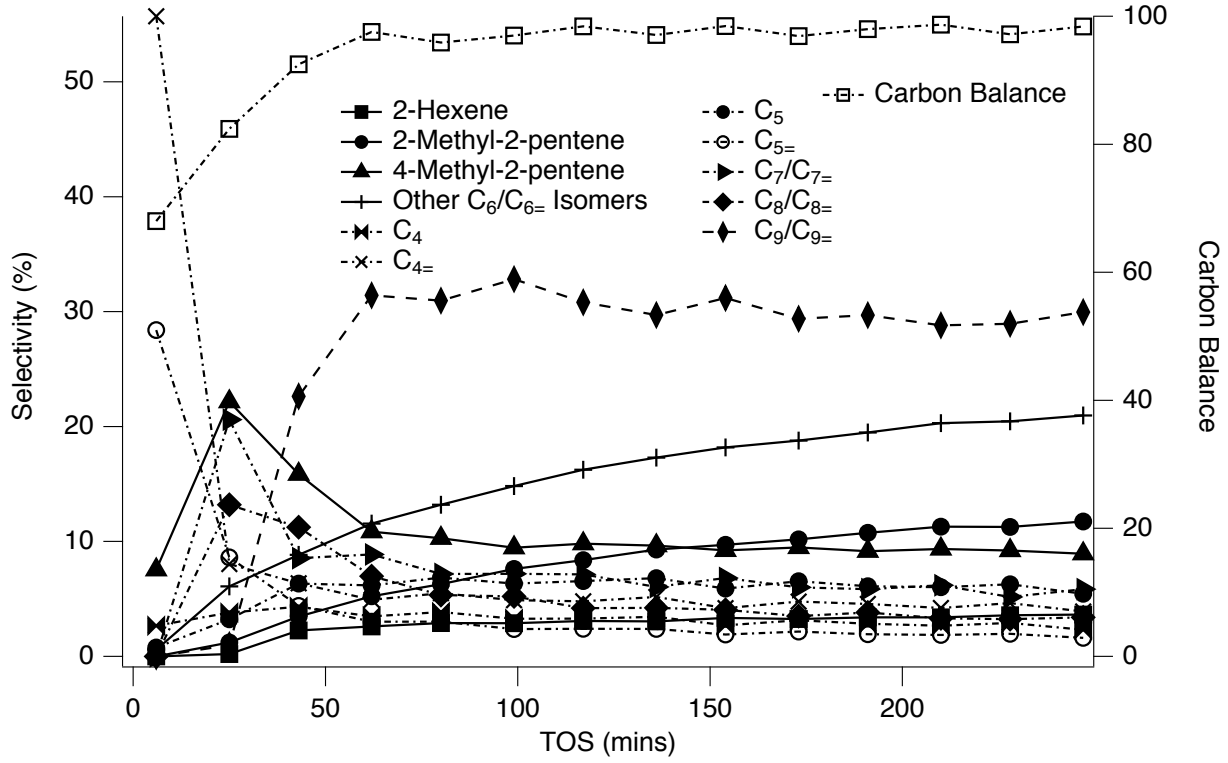

Figure S29. All Selectivities vs. TOS for Run #2 Ni-USY at 250 °C

Comparisons of Reaction Data at 180 °C and 250 °C For Ni-CIT-6 and Samples Exchanged with Mg^{2+} or Ca^{2+}, Calcined, and Ni^{2+}-Exchanged

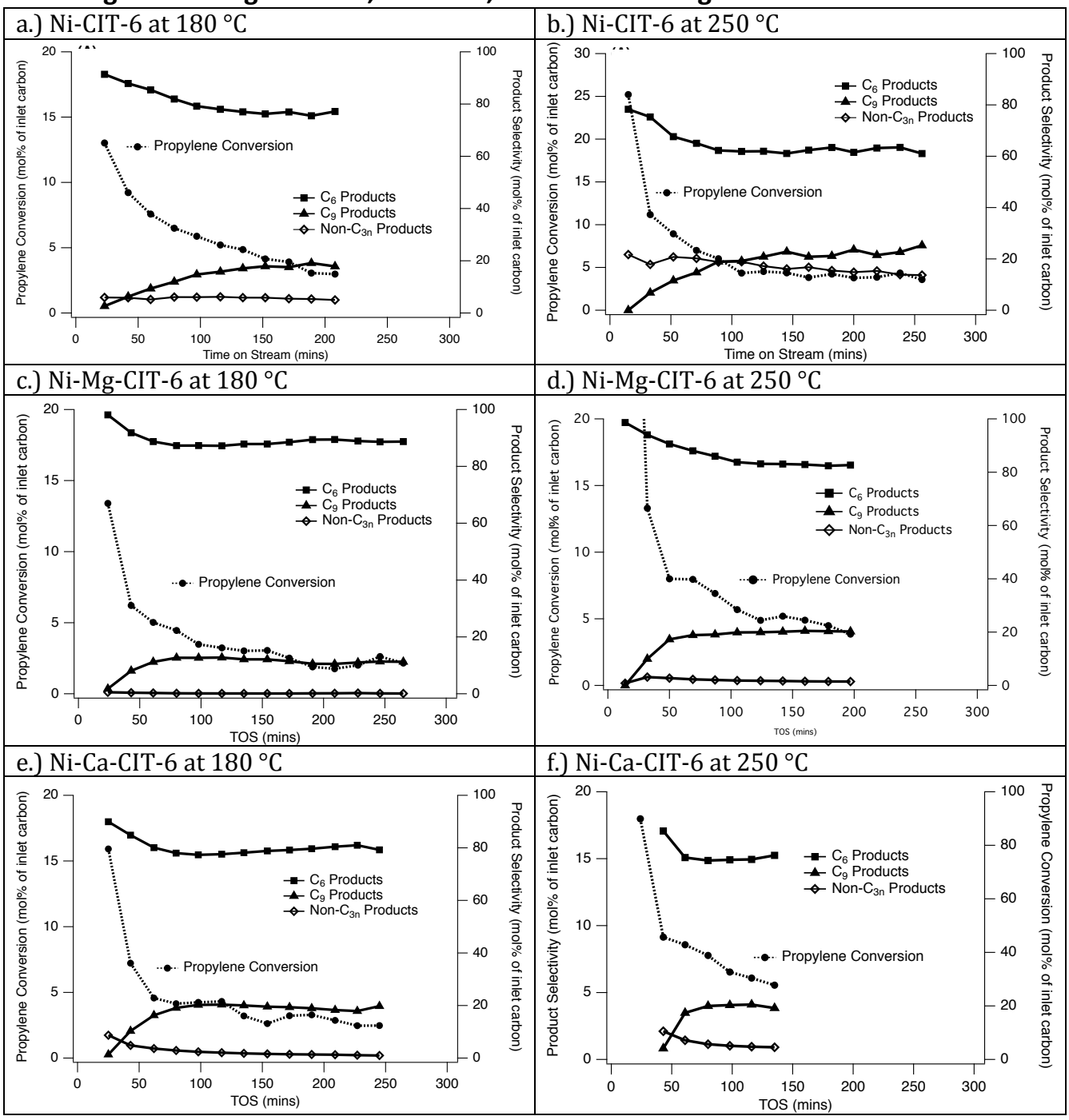

Figure S30. Reaction Comparisons for Ni-CIT-6, Ni-Mg-CIT-6, and Ni-Ca-CIT-6 at 180 °C and 250 °C

Post-Reaction Powder XRDs

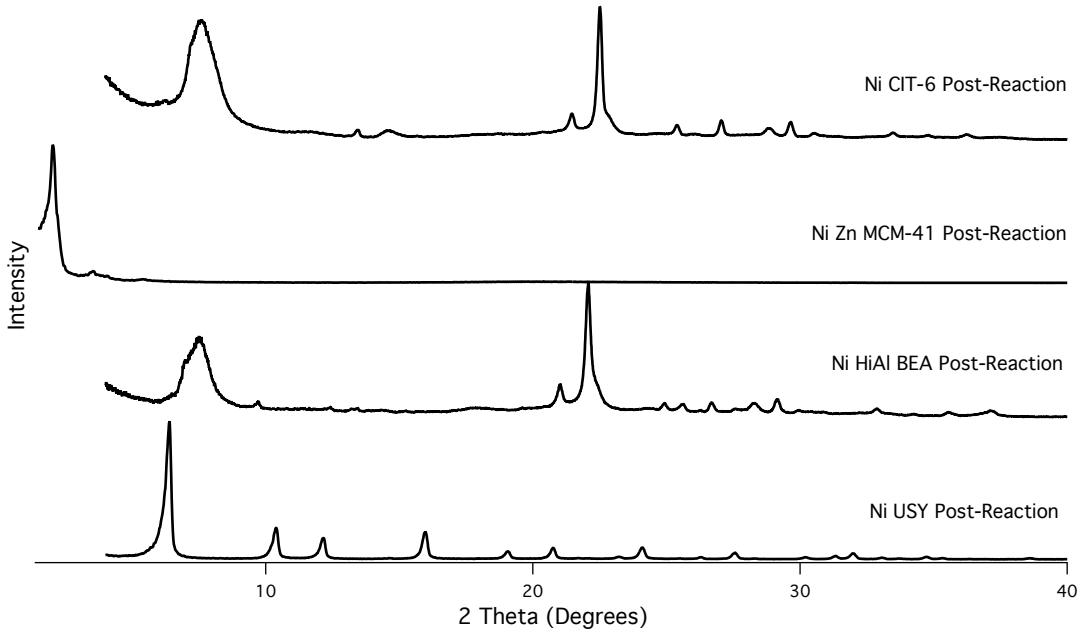

Figure S31. XRD Patterns for All Catalysts Post-Reaction

Post-Reaction TGAs of Spent Catalysts

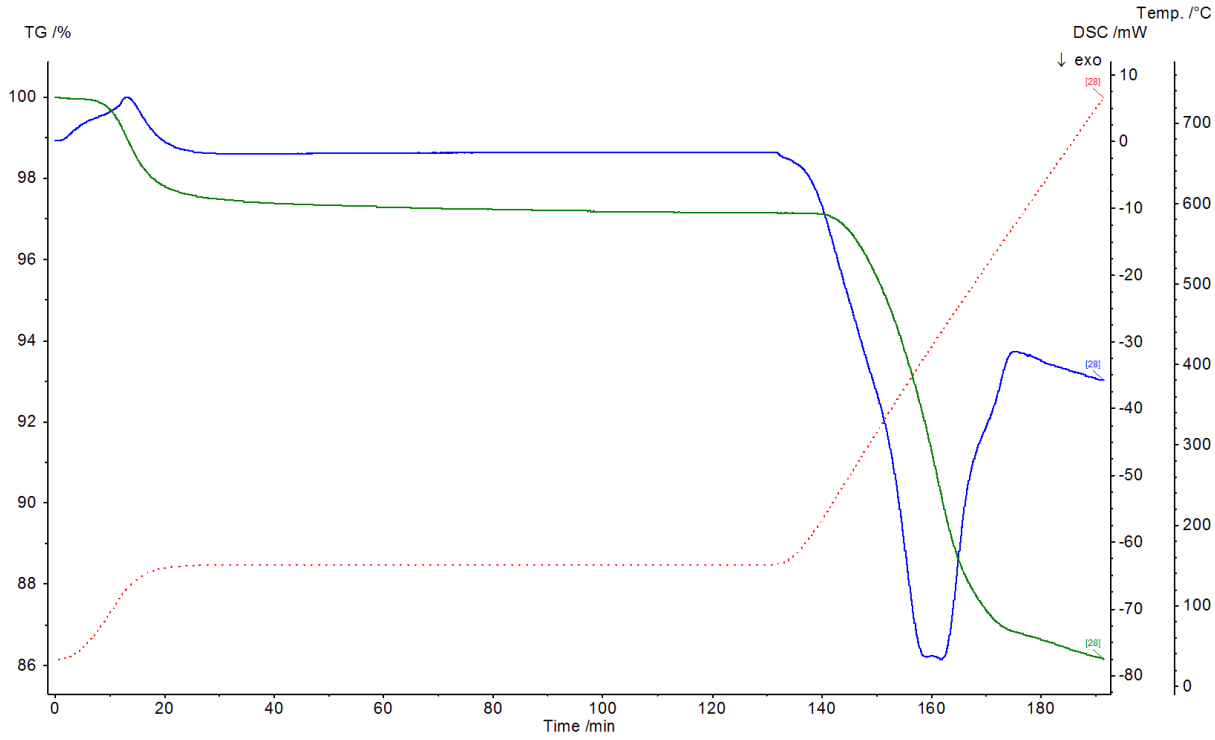

Figure S32. TGA for Ni-CIT-6 at 180 °C Post-Reactions

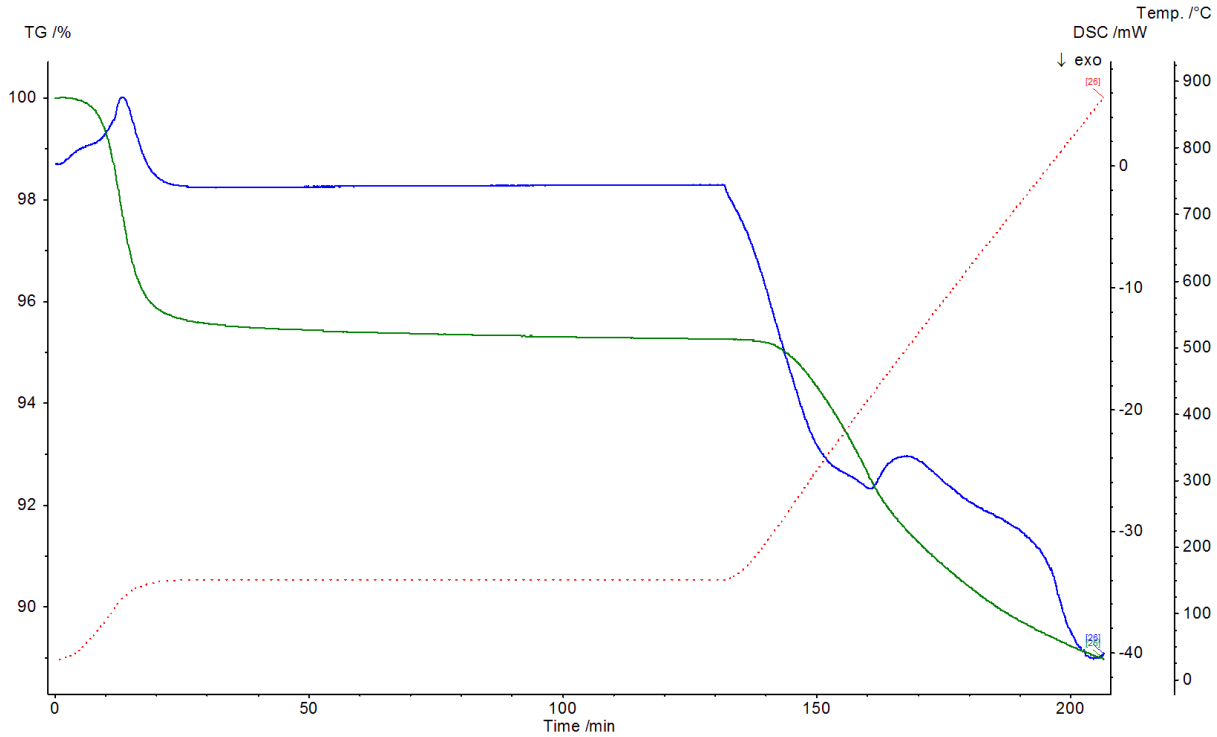

Figure S33. TGA for Ni-Zn-MCM-41 at 180 °C Post-Reactions

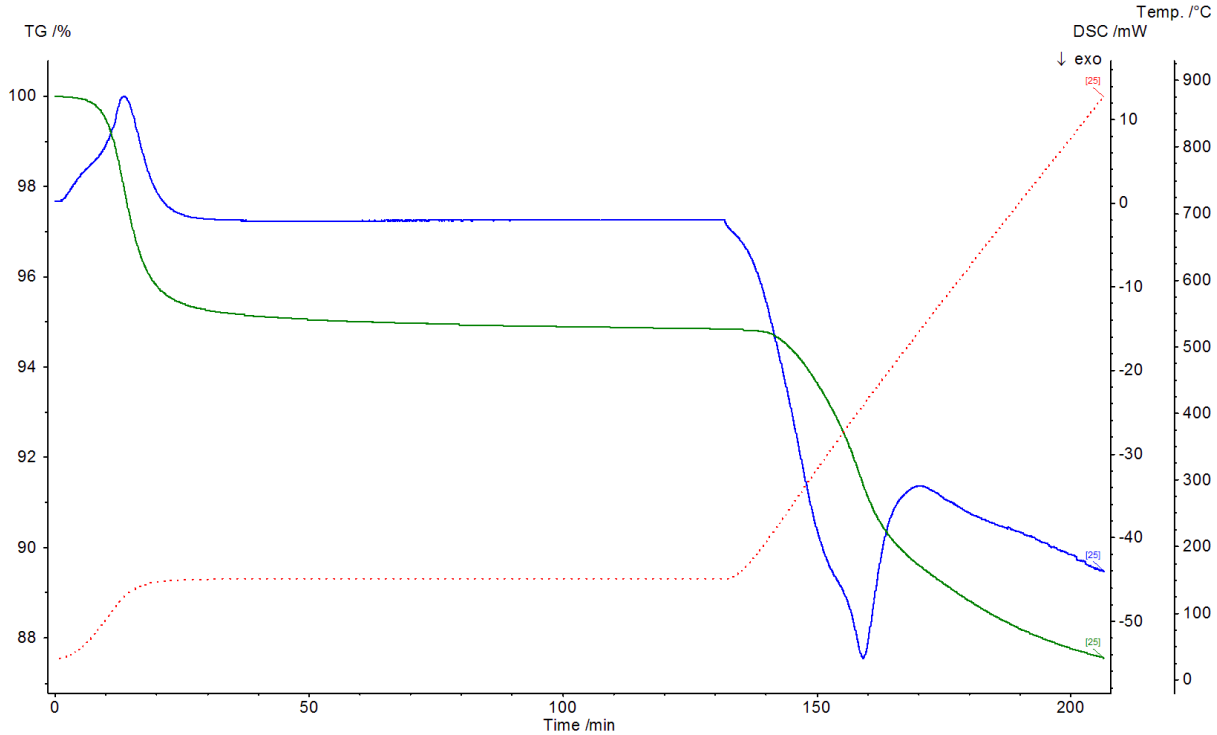

Figure S34. TGA for Ni-Zn-MCM-41 at 250 °C Post-Reactions

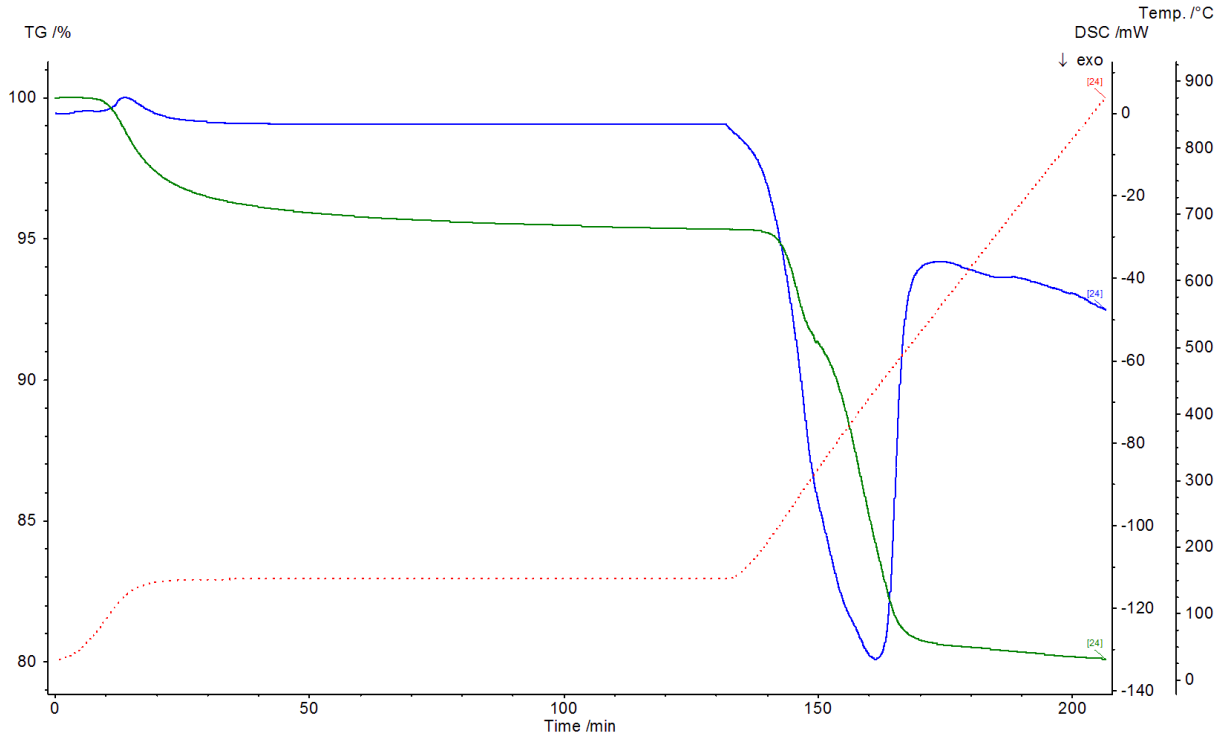

Figure S35. TGA for Ni-HiAl-BEA at 180 °C Post-Reactions

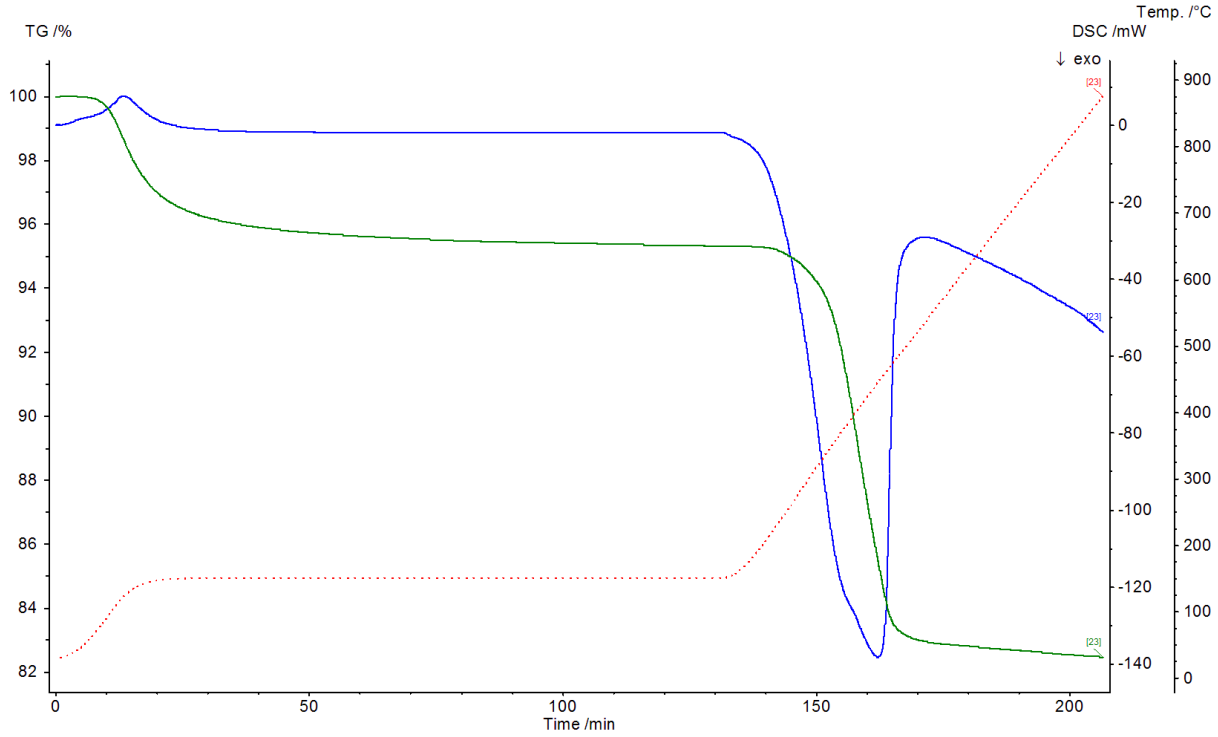

Figure S36. TGA for Ni-HiAl-BEA at 250 °C Post-Reactions

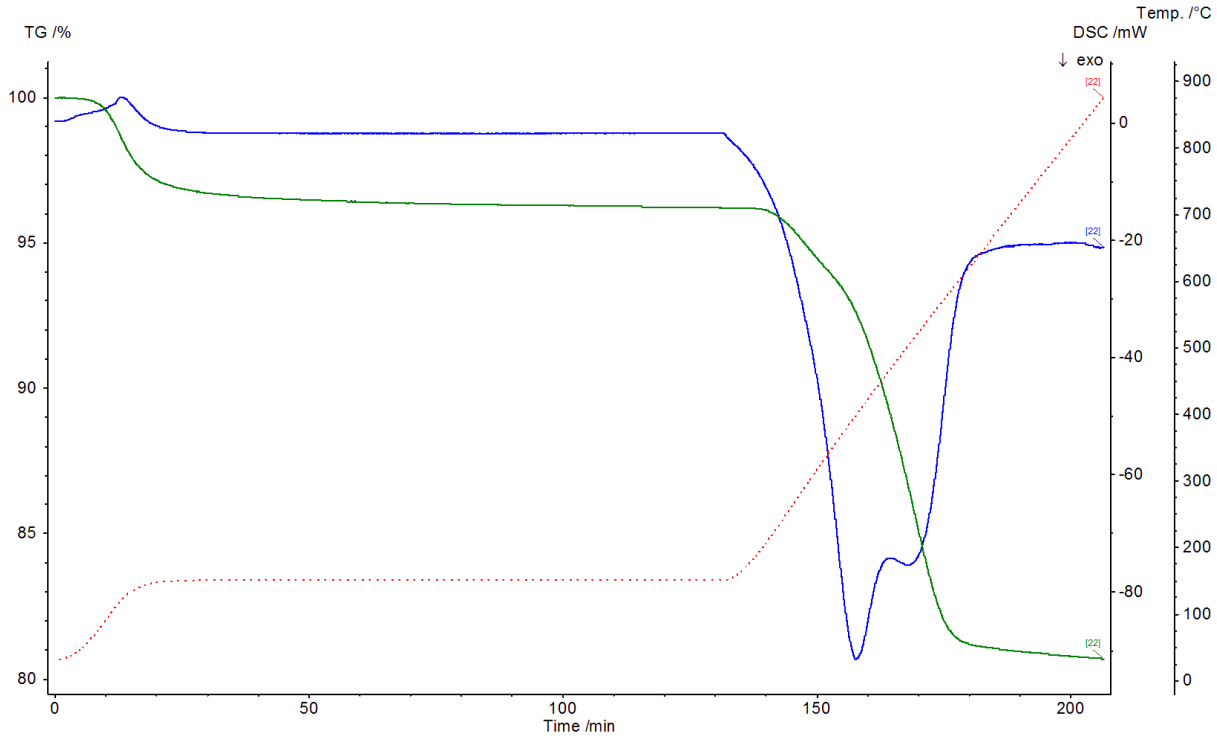

Figure S37. TGA for Ni-USY at 250 °C Post-Reactions